Entropically driven motion of polymers in nonuniform nanochannels

Tianxiang Su and Prashant K. Purohit

Phys. Rev. E **83**, 061906 — Published 7 June 2011

DOI: 10.1103/PhysRevE.83.061906

Entropically driven motion of polymers in non-uniform nanochannels

Tianxiang Su and Prashant K. Purohit*
Department of Mechanical Engineering and Applied Mechanics,
University of Pennsylvania, Philadelphia, Pennsylvania 19104, USA

In nanofluidic devices, non-uniform confinement induces an entropic force that automatically drives biopolymers towards less confined regions to gain entropy. To understand this phenomenon, we first analyze the diffusion of an entropy-driven particle system. The derived Fokker-Planck equation reveals an effective driving force as the negative gradient of the free energy. The derivation also shows that both the diffusion constant and drag coefficient are location dependent on an arbitrary free energy landscape. As an application, DNA motion and deformation in non-uniform channels are investigated. Typical solutions reveal large gradients of stress on the polymer where the channel width changes rapidly. Migration of DNA in several non-uniform channels is discussed.

Keywords: non-uniform nano-channel, entropic force, DNA rod model, DNA dynamics and deformation

I. INTRODUCTION

The development of techniques for confining DNA in nanofluidic channels has pushed genomic studies up to a new level. Researchers are now capable of using nanochannels to stretch a single DNA molecule, to sort DNAs based on their sizes, and to study repressor-DNA interactions, *etc* [1–4]. To interpret the experimental data, theorists have been developing models to predict the free energy, the average extension, relaxation time, *etc*, of a confined polymer [5–9]. Among those theories, the two most well-known in the field are those described by de Gennes [5] and by Odijk [6].

de Gennes' theory is applicable for a moderately confined polymer. The theory requires $D >> p$, where D is the channel width and p is the persistence length of the polymer. In this regime, DNA forms blob-like structures aligned along the channel. Evaluated at the average extension, the free energy G of the confined DNA scales as $G \sim D^{-5/3}$ in this regime [9, 10]. This tells us that, with the increase of the channel size, the free energy of the polymer decreases.

On the other hand, Odijk's theory studies a strongly confined polymer with $D << p$. In this regime, DNA is deflected back and forth by the channel walls, extending its backbone almost linearly inside the channel. Evaluated at the average extension $\langle \Delta z \rangle$, the free energy (per unit length) in this strong confinement regime takes the form [11]:

$$G\Big|_{\Delta z = \langle \Delta z \rangle} = \frac{c k_B T}{p^{1/3}\, D^{2/3}}, \tag{1}$$

where k_B is the Boltzmann constant, T is the absolute temperature and $c = 2.5$ is a constant for a cylindrical channel. This expression again suggests that the free energy is a decreasing function of D. The consequences of such a dependence of the free energy on the channel width are rarely investigated because many of the studies so far have focused on confining polymers in a uniform channel. However, in a non-uniform channel the dependence of G on D implies a free energy gradient, and therefore an effective driving force along the channel axis. This effective force can automatically drive the DNA to migrate along the channel without fluid flow or applied electric fields. Understanding this force can therefore help design new nanofluidic channels for better DNA manipulation.

The effective force described here is essentially an entropic force: by moving to a wider region inside a non-uniform channel, DNA experiences less confinement, gains more degrees of freedom and thus increases its entropy. This lowers the free energy of the system. Entropic forces of this kind can be found in problems like translocation of DNA through nanopores, where DNA is driven by an electric field, against an entropic force, to pass through a nanopore that separates two wide compartments [12, 13]. The entropic force acting on the DNA is revealed by the spontaneous retracting motion of the molecule when it is partly inserted into the nano-channel [14]. Such retracting motion was modelled by Mannion et al. [14] by performing a force balance where the drag force on the DNA due to the surrounding fluid counteracts a constant entropic force. For simplicity, evolution of the local deformation of the DNA during its motion was neglected in these studies. Aside from non-uniform confinement, entropic forces on translocating polymers can also arise from reversible binding of particles (proteins, for instance) on one end of the polymer chain, which creates the so-called entropic Langmuir pressure [15]. Entropic forces have also been reported to play a role in unfolding DNA molecules in channels [16]. In an even broader context, the widely studied diffusiophoresis phenomena on colloidal particles is also created by entropic forces [17–19].

The goals of this paper are (1) to understand the channel-shape dependence of the confinement induced entropic force on a polymer, and (2) to study the coupled migration and deformation of a polymer in a non-uniform channel. To understand the entropic force, we first study the diffusion of particles on a free energy landscape with

* Corresponding author: purohit@seas.upenn.edu

varying entropy. A Fokker-Planck equation is derived, which reveals an effective entropic force $f_{\rm ent} = -\nabla G$, automatically driving the system to reduce the free energy per particle G. The derivation also reveals that both the diffusion 'constant' and the drag coefficient become location-dependent as long as $\nabla G \neq 0$. Using the derived effective entropic force, we further study the motion and deformation of a polymer in a non-uniform channel. The problem is governed by a second order partial differential equation (PDE), whose solution gives both the migration velocity and the strain distribution along the polymer backbone.

Another issue arising in the context of a polymer confined in a non-uniform channel is the possible transition between the de Gennes' and Odijk's regimes. It is commonly acknowledged that the transition channel width for a stress free DNA is roughly $D \sim 50 - 100$nm, although more complex phenomena have been reported in this transition regime [20, 21]. As the polymer moves and deforms inside a non-uniform channel, stress can develop along its backbone so that the transition width is no longer $D \sim 50 - 100$nm. Even in a uniform channel, when electrical force is applied, the transition width is expected to increase. In this paper we estimate the transition width D as a function of the applied force so that we know roughly which theory to use based on the current location of the DNA and its local stress state. For simplicity, we will focus on a piece of DNA moving in a narrow non-uniform channel such that it is entirely in Odijk's regime. Then, we will discuss possible generalization of the theory to the de Gennes' regime.

II. ENTROPICALLY DRIVEN DIFFUSION

Before investigating the migration of DNA in non-uniform channels, we first briefly discuss entropically driven diffusion of particles in this section.

Consider a 1D random walk of an ensemble of particles on a free energy landscape with varying entropy (Fig. 1). Unlike in the classical random walk model, the particles considered here have different internal states. In free space where no spatial constraints are imposed, each particle has $\Omega_{\rm tot}$ internal states with energy E_i ($i = 1, 2, \cdots \Omega_{\rm tot}$). Along the z-axis, the 1D random walk domain, some spatially-varying constraints are imposed, reducing the number of accessible states for each particle to $\Omega(z) \leq \Omega_{\rm tot}$ at location z (Fig. 1). The spatial constraints are non-uniform and therefore $\Omega(z)$ depends on z. The particles are on an entropy-varying landscape. In the context of confined DNA in nano-channels, one can think of the different internal states as different configurations of the DNA. The non-penetration constraint posed by the non-uniform channel wall forbids some of the configurations and reduces the number of accessible states. We define the location dependent partition function as $\Xi(z) = \sum_{i=1}^{\Omega(z)} \exp(-\beta E_i)$, and the z-dependent free energy as $G(z) = -k_B T \log \Xi(z)$. Note that in defining the partition function and the free energy, we have assumed local equilibrium.

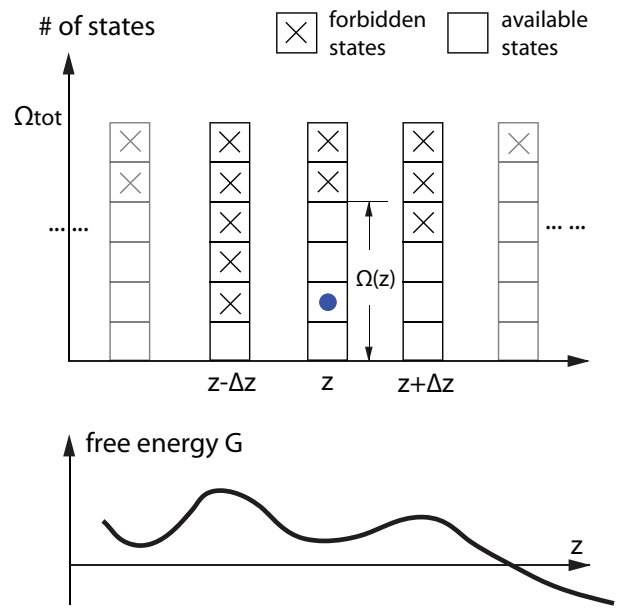

FIG. 1. (Color online) 1D random walk of particles (blue) in the z-direction. In its natural condition, each particle has $\Omega_{\rm tot}$ internal states ($\Omega_{\rm tot} = 6$ in the figure). Some z-dependent spatial constraints reduce the number of accessible states at location z to $\Omega(z) \leq \Omega_{\rm tot}$ (the blank boxes), creating an entropy varying landscape. Free energy is lower where there are more states to explore. An entropic force arises from this random walk model, driving the system towards regions with lower free energy.

One can derive the Fokker-Planck equation rigorously for this problem, which turns out to be:

$$\frac{\partial P}{\partial t} = \frac{\partial}{\partial z}\left[\mathcal{D}\frac{\partial P}{\partial z} - \left(\frac{-dG/dz}{\xi}\right)P\right], \qquad (2)$$

with $P(z,t)$ being the probability density for a particle being at location z at time t, $\mathcal{D}$ being the diffusion 'constant', and ξ being the drag coefficient.

Compared with the Fokker-Planck equation for a random walk with a 'real' applied force (say, by an optical tweezer or other instruments) [22], Eq. 2 reveals that the non-uniform spatial constraint creates an effective force $-dG/dz$, which drives the system towards regions with higher entropy to reduce the free energy. We note that free energy gradient has been shown to be a good approximation to the Langmuir pressure (an entropic force) in problems where ejection of DNA from bacteriophage is speeded up by the entropic effects of reversible binding of proteins in the host cell [15]. Here in our model, the free energy gradient is exactly, instead of approximately, the entropic force.

It is important to note that in an entropy-varying landscape, the diffusion 'constant' $\mathcal{D}$ is location-dependent:

$$\mathcal{D} \sim \Xi(z). \qquad (3)$$

This result comes out naturally in deriving the Fokker-Planck equation. It suggests that the particles diffuse faster where there are more states for exploration. This is analogous to the case of diffusion in porous media, where the effective diffusion constant is found to be proportional to the porosity of the media [23]. Furthermore, the Stokes-Einstein relation $\mathcal{D}\xi = k_B T$ implies that the drag coefficient ξ is also location-dependent when there are non-uniform spatial constraints. This is not surprising since it is well-known that the proximity of walls can change the drag coefficient on bodies in low Reynolds number flows [24].

Using conservation of mass: $P_{,t} = -J_{,z}$, we obtain from Eq. 2 the particle flux J as:

$$J = -\mathcal{D}\,\frac{\partial P}{\partial z} - \frac{dG/dz}{\xi}P. \tag{4}$$

An analytic steady state distribution can be found, even with both $\mathcal{D}$ and ξ being functions of z, by setting J to be a constant:

$$P_{\text{steady}}(z) = P_0\,\Xi(z)\int\frac{dz}{\Xi^2(z)}, \tag{5}$$

where we recall that $G(z) = -k_B T \log \Xi(z)$ and P_0 is a normalization constant. This is the steady state probability density of particles on an arbitrary free-energy landscape with a non-uniform diffusion constant. To verify if this solution is correct, we consider a random walk in $z \in [z_0, z_1]$ with $G(z) \propto \log(z)$. The boundary condition at $z = z_0$ is a hard wall, and at $z = z_1$ it is an absorption wall. Without any fitting, Eq. 5 agrees almost exactly with the result from a Kinetic Monte Carlo (KMC) simulation (Fig. 2). Here the KMC simulation was performed using the algorithms given in Voter [25].

Further, we note that the first term on the right-hand-side of Eq. 4 is the diffusive flux, while the second term is the drift flux $(v - v_{\text{fluid}})P$. Therefore, the mean velocity v of the system is:

$$v = v_{\text{fluid}} + \frac{f_{\text{app}} - dG/dz}{\xi}. \tag{6}$$

Here v_{fluid} is the fluid velocity and f_{app} is an external applied force. Eq. 6 is essentially an equation for force balance if, again, $-dG/dz$ is interpreted as an effective entropic force:

$$\underbrace{f_{\text{app}}}_{\text{external force}} + \underbrace{\left(-\frac{dG}{dz}\right)}_{\text{entropic force}} + \underbrace{\xi\,(v_{\text{fluid}} - v)}_{\text{drag force}} = 0. \tag{7}$$

Eq. 7 without the entropic force term has been used to model macromolecules stretched in fluid flow [26]. Here we show that a non-uniform spatial constraint gives rise to an effective entropic force term that must be included in the macroscopic force balance equation.

Interestingly, exactly the same results as presented above for particles in an entropy varying landscape can be derived by using another method – starting from the Sackur-Tetrode formula for the entropy of an ideal gas and considering the heat production rate. We show the derivation in Appendix A.

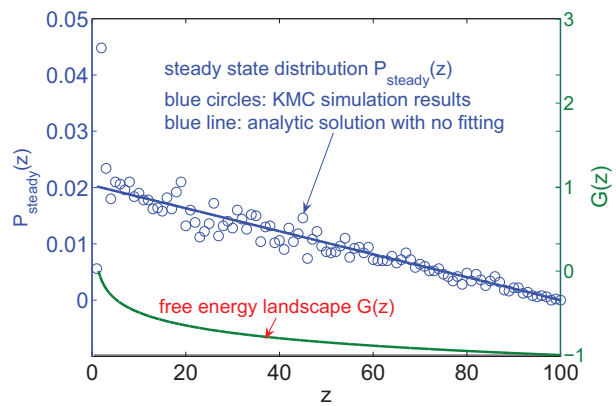

FIG. 2. (Color online) Steady state distribution $P_{\text{steady}}(z)$ (y-axis on the left) on a free energy landscape $G(z) \propto \log(z)$ (y-axis on the right). The random walk domain is $z \in [1, 100]$, with $z = 1$ being a hard wall and $z = 100$ being an absorption wall. Eq. 5 predicts a linear steady state distribution (blue line), which is confirmed, without any fitting, by the Kinetic Monte Carlo simulation results (blue circles). The numbers in this figure are in SI units.

III. DNA CONFINED IN NON-UNIFORM CHANNELS – THEORY AND COMPUTATION

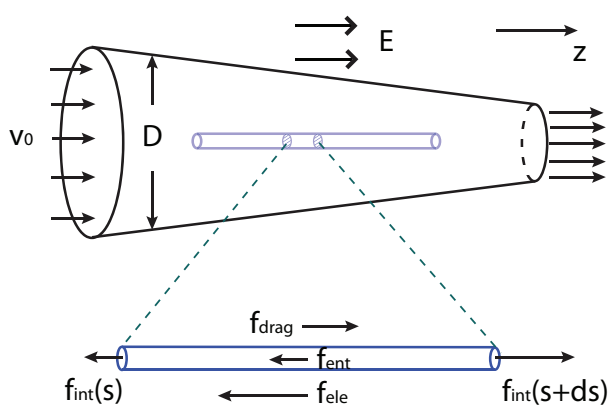

FIG. 3. (Color online) A DNA molecule is modelled as a 1D rod confined in a non-uniform channel. Typically, inside a nano-channel the DNA molecule can be subjected to stretching force f_{int}, drag force f_{drag} exerted by the surrounding fluid flow, entropic force f_{ent} due to the non-uniform confinement and also electrical force f_{ele} since the DNA is charged. The figure shows balance of force for an infinitesimal segment on the rod.

We now analyze the migration and deformation of a DNA molecule in a non-uniform channel. Under strong

confinement, a DNA molecule (or any semi-flexible polymer) can be modelled as a fluctuating 1D rod (Fig. 3) [26]. The rod is parametrized by its arc length $s \in [0, L]$, with L being the contour length of the polymer. We denote the location of the DNA inside the channel at time t as $z(s,t)$, so that $\partial z/\partial t = \dot{z}$ is the local velocity and $\partial z/\partial s = \lambda$ is the local stretch of the DNA. Note that $\dot{z} > 0$ if the polymer is moving from left to right (Fig. 3).

Below, we first analyze different forces that act on the polymer. Of particular interest are the entropic force and the drag force. As pointed out in the previous section, the free energy gradient $-dG/dz$ serves as an effective entropic force *per unit length* f_{ent}. Using Eq. 1, we obtain:

$$f_{\text{ent}} = \frac{5}{3}\frac{k_B T}{p^{1/3} D^{5/3}}\frac{dD}{dz}. \tag{8}$$

This entropic force is positive when $dD/dz > 0$. Therefore, it drives the system towards regions with higher entropy. Also, like other entropic forces in polymer science, it depends linearly on the thermal energy $k_B T$ [15, 22]. Moreover, its magnitude is governed not only by the gradient of the channel width, but also by the property of the polymer, like the persistence length p. A very stiff polymer with large persistence length p would be extended linearly along the channel without feeling much confinement. Therefore, the entropic force due to non-uniform confinement will be weak on stiff polymers. The total entropic force acting on the entire DNA can be estimated as:

$$\int_0^L (-dG/dz)ds \approx \frac{c\left[D^{-2/3}(0) - D^{-2/3}(L)\right]}{\beta\lambda p^{1/3}}. \tag{9}$$

Using Eq. 9, a divergent channel with $D(0) = 25$nm and $D(L) = 50$nm will pose a total entropic force of approximately 0.15pN on a strongly confined DNA with $\lambda \approx 0.8$ and $p = 50$nm. This force is significant because the typical thermal force scale on a DNA molecule is $k_B T/p \approx 0.08$pN.

Translating polymers in a nanochannel also experience a fluid drag. When the confinement is strong, hydrodynamic interactions between the polymers and the channel walls become important and cannot be neglected. For example, for a slender body of contour length L and radius a moving between two walls that are separated by a distance $D << L$, the longitudinal drag coefficient per unit length is [27]:

$$d_{t2} = \frac{2\pi\mu}{\log\left(D/a\right) - 0.453}\,, \tag{10}$$

with μ being the viscosity of the fluid. The subscript 2 stands for confinement by two walls. d_{t2} is much larger than $d_{t0} = \frac{2\pi\mu}{\log(L/2a)+c}$ with $c \approx \mathcal{O}(1)$, which is the drag cooefficient for the same slender body moving in a fluid with no nearby walls [24]. In our problem, a polymer in a nanochannel can be modelled as a slender body confined by four walls. Using superposition [28] and the fact that $d_{t2} >> d_{t0}$ [24], the drag coefficient for such a slender body is approximately:

$$d_t \approx \frac{4\pi\mu}{\log\left(D/a\right) - 0.453}. \tag{11}$$

It has been shown, by several independent studies, that the method of superposition for calculating the drag coefficient yields reasonably good agreement with experimental measurements [29–31], even though it is not exact.

To determine d_t, we still need to know the radius a of the slender body. Marko and Siggia [32] suggested that the effective radius should be taken as the transverse size $R_\perp$ of the elongated polymer. This depends not only on the width D of the channel, but also on the persistence length p of the polymer. Given the stretch λ of the polymer, we estimate $R_\perp$ in Appendix B, and the result is:

$$R_\perp = a_0\lambda + 0.7445\left(pD^2\right)^{1/3}\sqrt{1-\lambda^2}\,, \tag{12}$$

with $a_0 = 1.0$nm being the geometric width (radius) of a DNA molecule [33–35]. Since $\left(pD^2\right)^{1/3} >> a_0$, $R_\perp$ is a decreasing function of λ, which makes sense because for an inextensible rod, the perpendicular deflections should decrease as the stretch increases.

A substitution of $R_\perp$ into a in Eq. 11 suggests that a polymer with less transverse fluctuation experiences less drag. In particular, for $D = 50$nm, the drag coefficient per unit length is about 39.6 pN ms μm^{-2} at zero force. In comparison, it has been estimated that when there is no confinement, the drag coefficient is about 0.61 pN ms μm^{-2} for a DNA molecule [36]. In micron scale channels, on the other hand, the drag coefficient is about 1.2 pN ms μm^{-2} [36]. Our estimate shows that when the channel width is on the nanometer scale, the drag coefficient increases significantly. Further, we note that λ and $R_\perp$ depend on the internal stretching force f_{int} (discussed below in Eq. 14). Therefore, d_t is also a function of f_{int}. We show their relation in Fig. 4. As expected, increasing the stretching force reduces the transverse size of the polymer, which leads to a smaller d_t.

Next, we do a force balance on an infinitesimal segment of the rod, which, aside from the above mentioned two forces, also experiences (Fig. 3): (1) internal stretching force f_{int} exerted by its neighbouring segments, and (2) electrical force per unit length f_{ele} arising from the applied electric fields. Balance of forces in the longitudinal direction (Eq. 7) requires these forces sum to zero:

$$\frac{\partial f_{\text{int}}}{\partial s} - d_t\left(\frac{\partial z}{\partial t} - v_{\text{fluid}}\right) + f_{\text{ele}} + f_{\text{ent}} = 0. \tag{13}$$

In this force balance analysis, long-range hydrodynamic interactions between different material points on the DNA are neglected because the polymer is under strong confinement. A random force can be added, but, to study the average behavior, we do not include it in Eq. 13.

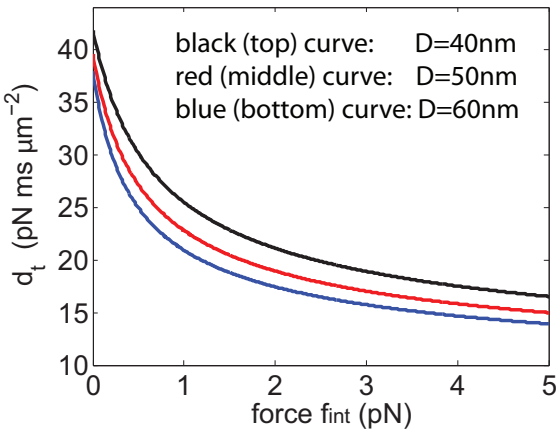

FIG. 4. (Color online) Drag coefficient per unit length as a function of the stretching force $f_{\rm int}$ at different channel widths D (calculated using Eq. 11, Eq. 12 and Eq. 14).

Also, since the Reynolds number is low in a nanofluidic channel, it is legitimate to ignore inertia. We also note that the drag force may also depend on the strain rate $\partial v_{\rm fluid}/\partial z$ [37], but in this study we neglect this effect. This is consistent with Eq. 7.

To solve for the two unknowns $z(s,t)$ and $f_{\rm int}(s,t)$, we also need a constitutive equation [26]. In particular, following Marko and Siggia [32], we will apply the constitutive relation locally on the polymer. For a strongly confined DNA, Wang and Gao [38] showed that the force-stretch relation is:

$$f_{\rm int} = \frac{1}{\beta p}\left[\frac{1}{4(1-\lambda)^2} - c^2\left(\frac{p}{D}\right)^{4/3}\right], \qquad (14)$$

where again $\lambda = \partial z/\partial s$ is the local stretch of the DNA and $c = 2.5$ is a constant for a cylindrical channel. Eq. 13 and Eq. 14 form the governing equations for the problem.

To identify the relative order of magnitude of each term in the governing equations, we scale the problem using the following non-dimensional quantities:

$$\bar{z} = \frac{z}{L}, \quad \bar{s} = \frac{s}{L}, \quad \bar{D} = \frac{D}{p}, \quad \bar{a}_0 = \frac{a_0}{p}, \qquad (15)$$

$$\bar{f}_{\rm int} = f_{\rm int}\beta p, \quad \bar{f}_{\rm ele} = f_{\rm ele}\left(\frac{3}{5}\beta p L\right), \qquad (16)$$

$$\bar{t} = \frac{5t}{3\beta d_{t*} p L^2}, \quad \bar{v}_{\rm fluid} = v_{\rm fluid}\left(\frac{3}{5}\beta d_{t*} p L\right). \qquad (17)$$

Here $d_{t*} = 4\pi\mu$ is the numerator of the drag coefficient d_t (Eq. 11). The scaling suggests that the typical time scale for the problem is on the order of $\tau \sim \beta d_{t*} p L^2 \approx 10$s for a DNA molecule about 20μm long in water with viscosity 10^{-3} Nsm^{-2}. For a wider micron scale channel, however, the time scale is expected to be smaller since the drag coefficient is smaller and the molecules move faster. As a comparison, the Rouse bead and spring model predicts the first-mode structural relaxation time τ_1 of a polymer chain as $\tau_1 = \beta\xi L^2$ [39], with ξ being the drag coefficient per bead. Using $\xi = d_t l$ and $l \sim p$, where l is the natural length of each spring, we recover the time scale τ for our governing equations. We note that, more generally, a stretched polymer has two different relaxation times, one in the longitudinal direction $\tau_\parallel$ and one in the transverse direction $\tau_\perp$ [40]. The time scale $\tau \sim \beta d_{t*} p L^2$ for our governing equations is for the deformation in the longitudinal direction because t appears in our equations as $\partial z/\partial t$.

The two governing equations for $z(s,t)$ and $f_{\rm int}(s,t)$ (Eq. 13 and Eq. 14) can be decoupled. By plugging the constitutive law into the equation for force balance, we can eliminate $\bar{f}_{\rm int}$ and the result is an evolution law for $\bar{z}(s,t)$:

$$H(\lambda)\frac{\partial \bar{z}}{\partial \bar{t}} = \frac{3}{10\left(1-\bar{\lambda}\right)^3}\frac{\partial \bar{\lambda}}{\partial \bar{s}} + \left(\frac{5\bar{\lambda}}{\bar{D}^{7/3}} + \frac{1}{\bar{D}^{5/3}}\right)\frac{d\bar{D}}{d\bar{z}} + \bar{\mathcal{V}}. \qquad (18)$$

Here, the function $H(\lambda) = \left[\log(\bar{D}/\bar{R}_\perp) - 0.453\right]^{-1}$ is the contribution of the polymer-wall hydrodynamic interaction. $\bar{\mathcal{V}} = H(\lambda)\bar{v}_{\rm fluid} + \bar{f}_{\rm ele}$ can be viewed as an effective flow that combines the actual drag force with the electrical force. Eq. 18 is the central equation for the problem because its solution gives the velocity $\partial z/\partial t$ and also the deformation $\lambda = \partial z/\partial s$ of the DNA inside a non-uniform channel.

It is possible to design a non-uniform channel in which a DNA molecule remains stationary. The key is to use the fluid flow and applied electric field to exactly balance the entropic force. The shape of this special channel can be determined by setting $\partial\bar{z}/\partial\bar{t} = 0$ in Eq. 18, so that what remains is an ordinary differential equation (ODE) for the channel shape $D = D(z)$. To see this, we note that all the three terms on the right-hand-side of Eq. 18 can be written as functions of D because (1) by setting $f_{\rm int} = 0$, $\bar{\lambda} = \bar{\lambda}(\bar{D})$ by the constitutive law, and (2) for an incompressible flow, $\bar{v} = \bar{v}(\bar{D})$ because of mass conservation. We do not set up the ODE here for the sake of brevity.

Eq. 18 does not have an analytical solution for most cases. To solve the problem numerically, we discretize the rod into segments and do force balance using the wormlike-chain constitutive relation (with effects of confinement) for each of them. The local velocity and stretch of each segment are determined using the method discussed above. The discrete version of our governing equations essentially constitutes a string of beads connected by wormlike-chain linkers.

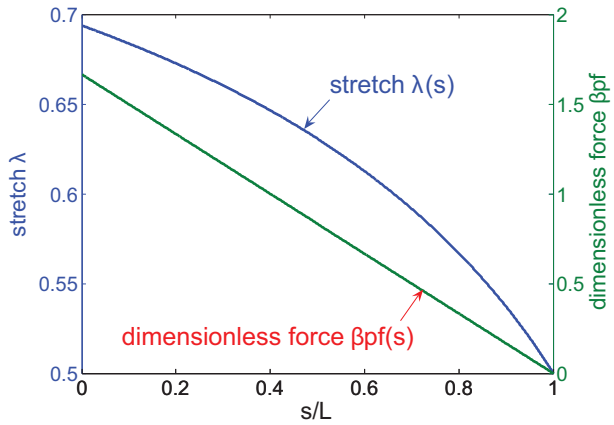

FIG. 5. (Color online) Stretch and force distributions along the arc length s of a stationary DNA in a uniform nanofluidic channel. The stretch distribution is non-linear: $(1-\bar{\lambda}) \sim (-\bar{s})^{-1/2}$ while the force distribution is always linear with slope being $-5\bar{\mathcal{V}}/3$.

IV. DNA CONFINED IN NON-UNIFORM CHANNELS – RESULTS

A. Stationary DNA in nanochannels

As the simplest special case, we first briefly discuss the results for a stationary DNA in a uniform channel. In this case, Eq. 18 reduces to:

$$\frac{\partial \bar{\lambda}}{\partial \bar{s}} = -\frac{10\bar{\mathcal{V}}}{3}\left(1-\bar{\lambda}\right)^3. \tag{19}$$

Assuming uniform flow, i.e, $\bar{\mathcal{V}}$ = constant is independent of $\bar{z}$ (since H depends weakly on λ, we neglect the dependence of H on λ here. When we do numerical simulations in the later discussions, this dependence will be taken into account), we get the analytic solutions:

$$\bar{\lambda}(\bar{s}) = 1 - \frac{1}{2\sqrt{A - \left(5\bar{\mathcal{V}}/3\right)\bar{s}}},\ \bar{f}_{\rm int}(\bar{s}) = -\frac{5\bar{\mathcal{V}}\bar{s}}{3} - \frac{c^2}{\bar{D}^{4/3}} + A. \tag{20}$$

Here $c = 2.5$ and A is a constant determined by the boundary condition. For example, $\bar{f}_{\rm int}(1) = 0$ for a free end leads to $A = 5\bar{\mathcal{V}}/3 + c^2\bar{D}^{-4/3}$.

The solution in Eq.20 suggests that the force distribution along the arc length is always linear while the stretch varies non-linearly as $(1-\bar{\lambda}) \sim (-\bar{s})^{-1/2}$ (Fig. 5). Moreover, when $\bar{\mathcal{V}} > 0$, both $\bar{f}_{\rm int}$ and $\bar{\lambda}$ are decreasing functions of $\bar{s}$. This implies that the strain along the DNA is highest at its 'upstream' end and lowest at its 'downstream' end, regardless of the boundary conditions posed. This is reasonable because forces applied at the 'upstream' end should balance the drag force along the entire DNA, so that the polymer can stay stationary.

B. Migration and deformation of DNA in non-uniform channels

We now analyze the entropy-driven migration of DNA in non-uniform channels. Firstly, we consider a channel with a sudden change in its width as shown in Fig. 6(a). Similar channels have been used to study the transport of DNA in nanopits [41], although in this section we will focus on channels narrow enough that the polymer is purely in Odijk's regime. The channel shape is modelled as a hyperbolic function $D(z) \sim \tanh(z/\eta)$, where η is a parameter characterizing the length scale over which the channel changes its width. As $\eta \to 0$, $D(z)$ becomes a step function.

To study the entropic effect, fluid flow and electric field are set to zero, so that the DNA is driven purely by the entropic force. We solve Eq. 18 numerically to obtain $z(s,t)$, with a stress-free initial condition $f_{\rm int}(s,0) = 0$ and stress-free boundary conditions $f_{\rm int}(0,t) = f_{\rm int}(L,t) = 0$. As expected, the DNA migrates to the wider region. The entire process can be divided into two stages, as explained in detail below.

Stage-(I): DNA moving across the interface $z = z_*$, at which the channel width changes (①–③ in Fig. 6). In this stage, the material point at the interface z_* experiences a large entropic force. Therefore, it moves with a larger velocity to the left compared to its neighbouring material points (see the enlarged figure in Fig. 6(a)). This stretches the material on the right of the interface and compresses the material on the left. As a result, a large force/strain gradient appears at the interface. This force/strain gradient travels along the DNA backbone as it moves across $z = z_*$, as shown in Fig. 6(b). This result implies that, if a polymer were to undergo structural change in a nano-channel, the change is most likely to occur at the interface where the channel shape changes most rapidly. Interestingly, some nanopores in cells, such as those in proteasomes, have indeed been found to cause structural changes in proteins [42, 43].

A second observation in this stage is that both ends of the DNA migrate at constant velocities (Fig. 7 shows the migration of the end $s = L$). This can be understood by looking into the central equation (Eq. 18). Before completely moving across the interface $z = z_*$, the stretch λ at both ends remains almost a constant and does not change with time. Therefore, Eq. 18 suggests an almost constant $\dot{z}$. This result holds even when there is fluid flow in the channel ($\bar{\mathcal{V}} \neq 0$). Our results also show a decrease in the total extension of the DNA in this stage (Fig. 6(c) ①–③). This is expected because during the migration, a larger portion of the DNA moves into the wider region, where it suffers less stretch.

Stage-(II): DNA leaving the interface (③–④ in Fig. 6). As the entire DNA molecule enters into the wider part of the channel, the force/strain gradient slowly relaxes and finally disappears (Fig. 6(b)). At the same time, the total extension of the polymer stops decreasing, and increases to reach an equilibrium value (Fig. 6(c)).

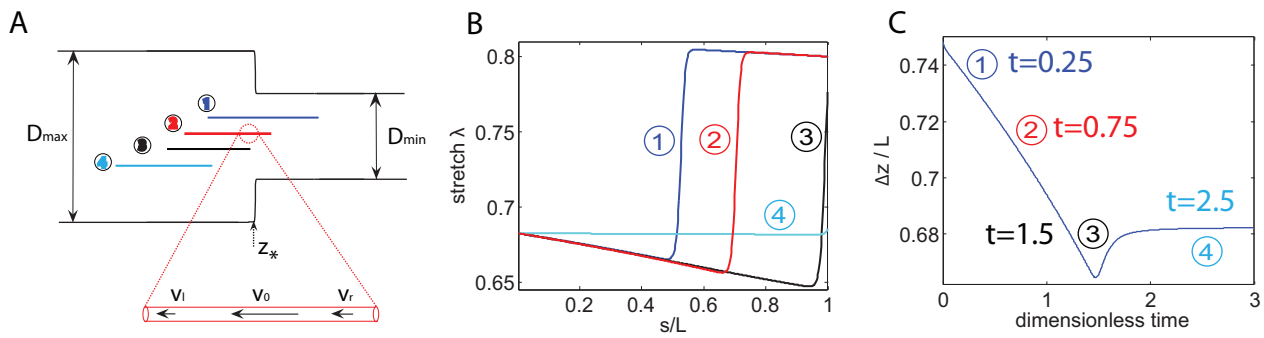

FIG. 6. (Color online) Entropically driven DNA crossing a sharp interface where the channel width changes suddenly. The channel shape is shown in (a). No fluid flow or electrical force is applied, so the DNA is driven only by the entropic force. The numbers in the circles represent snapshots of the molecule at different times. The process can be divided into two stages. Stage-(I): DNA moving across the interface at $z = z_*$ (① – ③). In this stage, a large force/strain gradient occurs at $z = z_*$ as is apparent in (b). This force/strain gradient is caused by the migration speed gradient as shown in the enlarged figure in (a) ($v_0 > v_l$, $v_0 > v_r$). The strain gradient travels along the DNA backbone until it completely enters into the wider region. Total extension of the DNA decreases in this stage as is apparent in (c). Stage-(II): DNA leaving the interface (③ – ④). In this stage, the force/strain gradient slowly relaxes as is apparent in (b). The total extension of the DNA stops decreasing, instead, it increases to reach an equilibrium value as is apparent in (c).

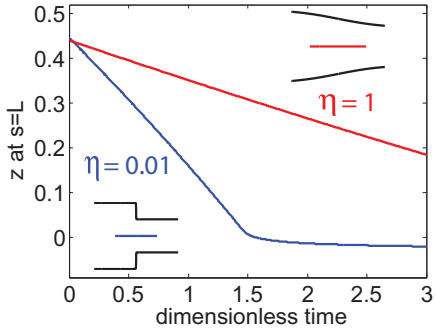

FIG. 7. (Color online) Movement of the right end of the DNA ($z(L,t)$ as a function of t) in channels with different η. No fluid flow or electrical force is applied, so the DNA is driven only by the entropic force. For a channel that changes its shape more rapidly (smaller $\eta = 0.01$, blue), the DNA moves faster because of larger entropic force. The initial condition is a stress free state. The boundary conditions are $f_{\text{int}} = 0$ at $s = 0$ and $s = L$.

Smoothing the change in width of the channel by increasing η can reduce the entropic force. Therefore, DNA is expected to migrate slower in a channel with a gently varying cross-section. This is confirmed by the solution to the central equation (Eq. 18). In Fig. 7, $z(L,t)$ is plotted for DNA in two different channels with $\eta = 0.01$ and 1 respectively, to show the velocity difference. No fluid flow is applied and the electrical force is set to zero.

Other more complicated non-uniform channels have also been fabricated in recent years, although most of them are at the micron scale [36]. We show the migration of a piece of DNA in four different types of such channels (in nanoscale so that the polymer is in Odijk's regime) in Fig. 8. The channel shape is $D(z) = (az+b)^n$, with $n = 1, -1/2, -2$ and -1 for the four channels. a and b are two constant parameters. No fluid flow or electrical force is applied, so the DNA is driven only by the entropic force. Our results suggest that with the same entrance width and exit width, a linear channel with $n = 1$ drives the polymer to move most slowly and the polymer suffers less stretch in this channel type (Fig. 8).

We next consider symmetric channels with two shape-changing regions as shown in Fig. 9(a) and (d). Again, the fluid velocity and electrical force are set to zero. These channels can exert entropic pulling and pushing forces on the molecule. In the channel shown in Fig. 9(a), the two ends are wider while the middle region is narrower. This creates a pair of pulling entropic forces on the confined polymer. Therefore, even without fluid flow or electrical force, stress/strain along the backbone quickly builds up and reaches a maximum in the middle where the confinement is stronger (Fig. 9(b)). The total extension of the polymer increases in response to the opposite entropic stretching and achieves equilibrium after some time as the polymer reaches a stationary state (Fig. 9(c)).

Fig. 9(d) is another symmetric channel with two narrow ends and a wide middle region. In this case, the entropic forces push the DNA into the middle region. However, as the DNA contracts, negative force builds up along the backbone, pushing against the entropic force until force balance is established (Fig. 9(e)). During the process, total extension of the polymer decreases in response to the entropic pushing (Fig. 9(f)). Again, we see large stress/strain gradients at the regions where the channel changes its shape.

A fluid flow or an applied electric field in the channel shown in Fig. 9(a) can break the symmetry of the problem. The DNA now migrates in response to the flow, or the electric field, through the nano-channel. The results with $v_{\text{fluid}} > 0$ and $f_{\text{ele}} = 0$ are shown in Fig. 10(b).

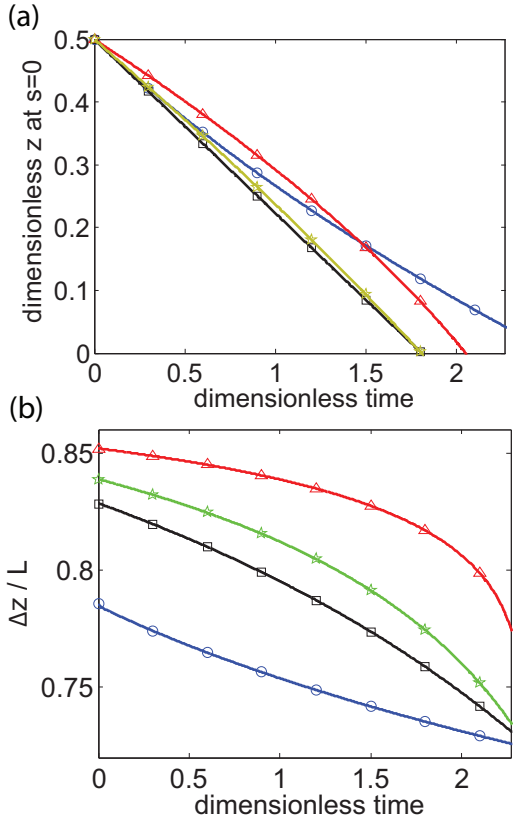

FIG. 8. (Color online) Migration of a piece of DNA in different types of nanochannels. The polymer is driven purely by entropic forces ($\bar{\mathcal{V}} = 0$). (a) $\bar{z}$ at $\bar{s} = 0$ versus dimensionless time. (b) Total stretch $\Delta z/L = [z(L) - z(0)]/L$ versus dimensionless time. Different lines are for different channel shapes $D(z)$. Blue circles: linear channel with $D(z) = az + b$. Red triangles: $D(z) = (az+b)^{-1/2}$. Black squares: $D(z) = (az+b)^{-2}$. Cyan stars: $D(z) = (az+b)^{-1}$. Here a and b are different constants for different channel types. For comparison, a and b for each channel type are chosen so that the entrance/exit widths of the four channels are the same.

The total stretch of the DNA increases as the polymer squeezes through the narrow region (Fig. 10(b)). Two force/strain gradients travel along the backbone of the DNA sequentially during the entire process (Fig. 10(c)).

Finally, we also investigate the dependence of the migration speed on the polymer contour length L and persistence length p. Three polymers with different contour lengths and persistence lengths ($L = 8$, 3 and 8μm, $p = 50$, 50 and 100nm respectively) are placed in a periodic channel with fluid flow $v_{\text{fluid}} > 0$ (Fig. 11(a)). Electrical field is again set to zero. Our results show that longer DNA moves faster in the periodic channel. At $t = 5$s, the long DNA with $L = 8\mu$m has already been separated from the short DNA with $L = 3\mu$m by $6 - 7$ microns (Fig. 11(b)). Changing the persistence length of the polymer does not significantly affect the migration velocity, at least in the case we studied. Fig. 11(b) shows that a polymer with $p = 50$nm migrates as fast as one with $p = 100$nm. This can be explained in the following way. Increasing the persistence length has two effects. Firstly, it reduces the drag coefficient since the effective radius of the polymer rod is less. This speeds up the migration. Secondly, it also reduces the entropic force (Eq. 8), which drives the polymer motion. This lowers the migration velocity. These two effects cancel each other, making the migration velocity not significantly dependent on the persistence length.

C. Transition to the de Gennes regime under non-zero force

The framework described above can be generalized to the de Gennes' regime by (1) adding proper force terms in the force balance equation (Eq. 13) since for a moderately confined DNA, volume exclusion effect and also the hydrodynamic force cannot be neglected any more, (2) changing the constitutive law for a blob-like polymer. To completely solve the problem of DNA in non-uniform channel, we also need to know at which channel width D the transition from the Odijk to de Gennes regime occurs. Although it is well-known that transition for a stress free DNA happens at channel width about $50 - 100$nm, transition width for a DNA under finite stress is unknown. Below we try to estimate the transition width between the two regimes as a function of the force.

We shall find the transition width in the following way. Odijk's theory assumes that under strong confinement, the angle fluctuation of the polymer is small such that second order approximation is proper. We shall find, in the $f - D$ plane, regions where the small angle approximation is valid. The other regions of the $f - D$ plane where small angle approximation is not valid are assumed to be in de Gennes' regime.

Let $\theta(s)$ be the angle formed by the polymer with respect to the axis of the channel. In the Odijk regime, using the small angle quadratic approximation, the mean angle fluctuation of a confined chain under end-to-end force f is found to be [38]:

$$\langle \theta^2 \rangle = \frac{1}{\sqrt{\beta p f + c^2 \left(p/D\right)^{4/3}}}, \tag{21}$$

In deriving this result, $\cos\theta \approx 1 - \theta^2/2$ was used. The ratio between the dropped quartic term $\theta^4/24$ and the retained quadratic term $\theta^2/2$ is:

$$e = \frac{\theta^4/24}{\theta^2/2} = \frac{\theta^2}{12}. \tag{22}$$

In order for the theory to be self-consistent, we need e to be small. Therefore, we try to find the regions on the $f - D$ plane where e is small and assume the rest of the plane corresponds to the deGennes' regime. The

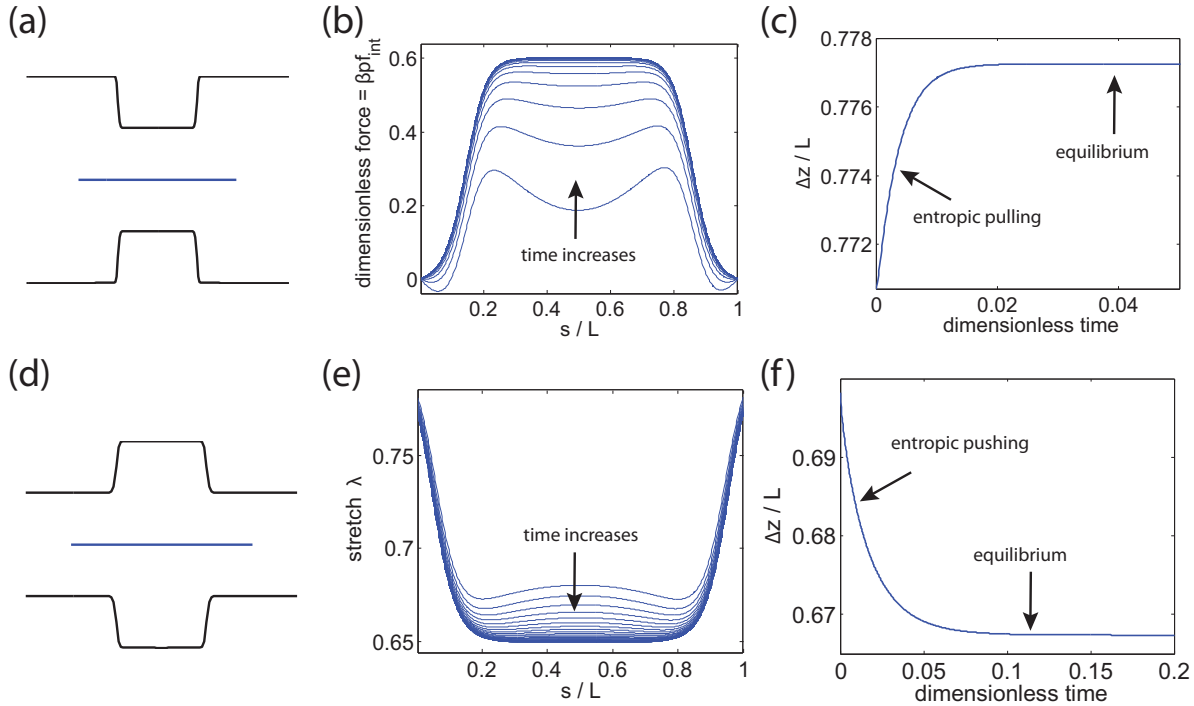

FIG. 9. (Color online) Motion and deformation of a piece of DNA in symmetric non-uniform channels without fluid flow or applied electric fields. (a–c): In the symmetric channel shown in (a), the initially stress-free polymer is pulled by a pair of entropic forces created by the channel. As a result, force and strain build up along the polymer backbone. In particular, large force gradient occurs at locations where the channel changes its shape most rapidly (b). The total extension of the polymer increases initially in response to the entropic pulling and then reaches equilibrium (c). (d–f): The symmetric channel shown in (d) creates a pair of entropic forces, which pushes the DNA inwards. In response, strain is developed along the polymer backbone (e). The total extension of the DNA decreases because of the pushing and then reaches equilibrium (f).

expression for $\langle e \rangle$ as a function of f and D is:

$$\langle e \rangle = \frac{\langle \theta^2 \rangle}{12} = \frac{1}{12\sqrt{\beta f p + c^2 \left(p/D\right)^{4/3}}}. \qquad (23)$$

We plot on the $f - D$ plane curves corresponding to $e = 3\%$ and 5% respectively in Fig. 12. For the region with e less than 3%, we claim the polymer is in Odijk's regime, for the zone with error larger than 5%, the polymer is more likely to be in de Gennes' regime. In between, there is uncertainty as to which regime best describes the behavior of the DNA. In fact, complex phenomena have been reported in the transition regions even when $f = 0$ [20, 21]. Fig. 12 shows that the transition occurs at wider channel width as the stress in the DNA increases. At $f = 0$, the transition width is around $50 - 100$nm, as expected.

V. CONCLUSIONS

The configuration and deformation of a confined polymer molecule depends on the channel width. But a non-uniform channel width results in more than a non-uniform deformation along the polymer. It actually drives the polymer to move in a direction perpendicular to the confinement. The driving force is entropic in essence, and it is revealed by a random walk model as $f_{\text{ent}} = -\nabla G$. The negative sign indicates that the force is driving the system to minimize its free energy. Including this force in the force balance analysis, we study the coupled deformation and motion of a piece of DNA in a non-uniform channel. The problem is governed by a second order PDE, whose solutions give the migration velocity and also the strain distribution along the polymer. DNA in different channel shapes are analyzed. A common feature is that large stress gradient occurs where the channel width changes dramatically. Longer DNA migrates faster through a nanochannel with fluid flow while the persistence length seems to have little effect on the migration velocity. Transition from Odijk's to de Gennes' regimes can occur in a non-uniform channel and is shown to be delayed if the stress along the polymer is high.

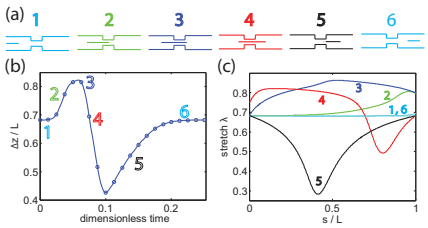

FIG. 10. (Color online) (a) A piece of DNA migrates along a non-uniform nano-channel with fluid flow $\bar{\mathcal{V}} > 0$. The numbers 1,2,3,4,5,6 represent snapshots in time. (b) Total stretch of the DNA increases as the polymer squeezes through the middle narrow region of the channel. (c) Two strain/stress gradients travel through the polymer backbone sequentially because there are two locations where the width of the channel varies rapidly.

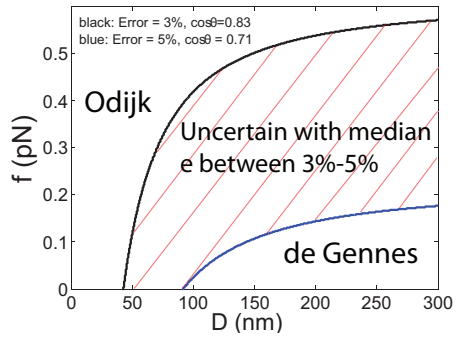

FIG. 12. (Color online) Transition between Odijk's and de Gennes' regimes. The two curves on the $f - D$ plane correspond to errors $e = 3\%$ (black), and 5% (blue) respectively. Region to the left of the curves is with less error. For the region with $e < 3\%$, we claim the polymer is in Odijk's regime. On the other hand, for the region with $e > 5\%$, the polymer is more likely to be in de Gennes' regime. We define 3%–5% as an uncertain zone, where transition between the two regimes occurs. The transition channel width is shown to increase with the increase of force.

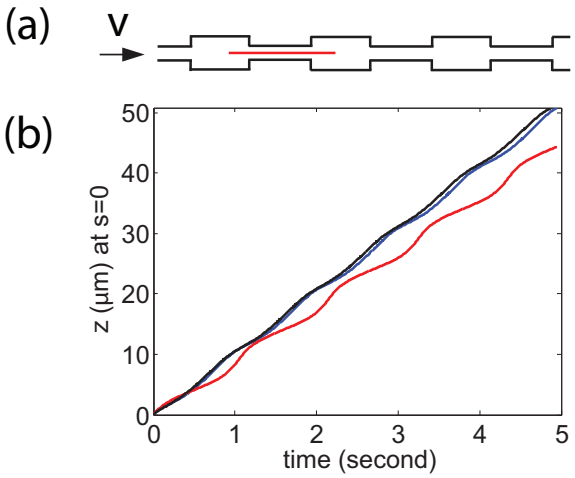

FIG. 11. (Color online) Migration of three different pieces of DNA in a periodic channel as shown in (a) (width in the wide/narrow region is $D = 50$nm and $D = 25$nm respectively, only one DNA molecule is shown). No electrical force is applied. Fluid in the channel flows to the right $v_{\text{fluid}} > 0$. (b) z at $s = 0$ versus time. Blue: $L = 8\mu$m, $p = 50$nm. Red: $L = 3\mu$m, $p = 50$nm. Black: $L = 8\mu$m, $p = 100$nm. At $t = 5s$, the long DNA (blue) and the short DNA (red) have been separated by 6.6 microns.

Appendix A: Results of entropy-induced migration derived from the Sackur-Tetrode equation

The conclusions drawn from the random walk model in the main text can be understood from a different point of view by considering the heat production rate of the system. In this section, we show that exactly the same results can be re-derived using the Sackur-Tetrode formula for the entropy of ideal gases.

Again, we imagine N particles diffusing on the z axis. In any infinitesimal interval dz, there are $NP(z)dz$ number of particles, where $P(z)$ is the particle density distribution. Using the Sackur-Tetrode formula [44], the entropy at position z can be written as:

$$\begin{aligned} S(z) = NP(z)k_B \log\left[\frac{V(z)}{h^3}\left(2\pi m k_B T\right)^{3/2}\right] \\ - NP(z)k_B \log\left[NP(z)\right] + \frac{5}{2}NP(z)k_B, \end{aligned} \tag{A1}$$

where h is the Planck constant and m is the mass of an individual particle. Note that the second term on the right-hand-side is the Boltzmann entropy for a probability distribution P, arising from the Gibbs' correction to the entropy of an ideal gas and will eventually lead to pure diffusion, as we shall show later.

Heat production rate of the system can be evaluated using Eq. A1, conservation of mass: $P_{,t} = -J_{,z}$ and integration by parts with boundary conditions $J(\pm\infty) = 0$. The result turns out to be:

$$\dot{Q} = T\frac{\partial}{\partial t}\int_z S(z)dz \tag{A2}$$

$$= Nk_BT\int_z \left[\frac{d\ (\log V)}{dz} - \frac{\partial P/\partial z}{P}\right] J\, dz. \tag{A3}$$

On the other hand, heat generation can be evaluated using the local power density [45]: $w = P(\xi J/P)(J/P) = \xi J^2/P$:

$$\dot{Q} = N\int_z \frac{\xi J^2}{P}\, dz. \tag{A4}$$

A comparison between Eq. A3 and Eq. A4 yields:

$$J = -\mathcal{D}\frac{\partial P}{\partial z} + \frac{-dG/dz}{\xi}P, \tag{A5}$$

where $dG = -k_B T d(\log V)$ has been used as the gradient of the free energy for a *single* particle under the condition that temperature is a constant [44]. This result agrees exactly with the one obtained from the microscopic model (Eq. 4). Plugged into the mass conservation law, Eq. A5 gives the evolution law for $P(z,t)$ shown in Eq. 2. We note that the first term in Eq. A5 is pure diffusion and it comes from the Boltzmann entropy for a probability distribution P in Eq. A1.

Compared to the random walk model, the theory discussed here considers the problem from a different point of view. Here a non-uniform entropy/free energy landscape causes heat production when a particle flux sweeps through. This contributes to the system as a source of heat. The framework for this model has been used to derive equations for thermal diffusion problems where a temperature gradient drives the diffusion of ideal gas [45]. Here we have used it for diffusion in an entropy-varying landscape.

Appendix B: Transverse size of a strongly confined polymer

Given a polymer under uniform stretch $\lambda = \partial z/\partial s$ inside a nano-channel of width D, we estimate the transverse displacement $R_\perp$ of the polymer in this section.

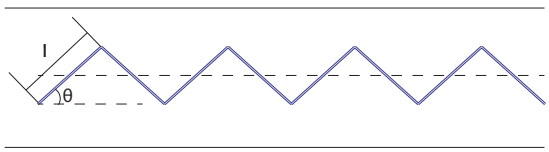

FIG. 13. Given θ, we find the l that minimizes the energy of the confined chain.

Since the stretch λ is uniform, for an inextensible chain, the tangent angle θ (the absolute value) is a constant along the contour. Therefore, the configuration of the polymer, modeled as a chain of links, is piece-wise linear, as shown in Fig. 13. There is only one free parameter for this configuration: l which is the length of each piece-wise linear segment. Below, we find $l_{\min}$ that minimizes the energy of the chain, from which we can obtain the transverse displacement as a function of the stretch. The energy per unit length of the chain is:

$$E = E_b + E_c + E_p = \frac{2K_b\theta^2}{l^2} + \frac{\Xi\theta^2}{24}l^2 + \frac{1}{2}f\theta^2, \tag{B1}$$

where K_b is the bending energy, Ξ is the quadratic confinement potential [38], and f is the applied force. The $l_{\min}$ that minimizes this energy is:

$$l_{\min} = \left(\frac{48K_b}{\Xi}\right)^{1/4}. \tag{B2}$$

Plugging in the relation between Ξ and D [38], we have the scaling relation: $l_{\min} \sim p^{1/3}D^{2/3}$, which agrees exactly with the prediction of Odijk and that of Burkhardt [6, 11, 46].

For the transverse displacement at the nodes (Fig. 13), we have: $R_\perp = \sin\theta l/2 + a_0\cos\theta$, where a_0 is the effective width of the DNA molecule without fluctuation. Therefore, the transverse displacement $R_\perp$ that minimizes the energy is:

$$R_\perp = a_0\frac{\partial z}{\partial s} + \left(\frac{3K_b}{\Xi}\right)^{1/4}\sqrt{1-\left(\frac{\partial z}{\partial s}\right)^2}. \tag{B3}$$

When $\partial z/\partial s = 1$, there is no thermal fluctuation, so the minimizer $R_\perp = a_0$, as expected. Plugging in the relation between Ξ and D [38], we obtain:

$$R_\perp = a_0\lambda + 0.7445\left(pD^2\right)^{1/3}\sqrt{1-\lambda^2}. \tag{B4}$$

ACKNOWLEDGMENTS

We acknowledge support from the Nano/Bio Interface Center at the University of Pennsylvania through the National Science Foundation NSEC DMR08-32802 and an NSF CAREER award grant number NSF CMMI-0953548.

[1] Q.F. Xia, K.J. Morton, R.H. Austin and S.Y. Chou, Nano. Lett. **8**, 3830 (2008).
[2] R. Riehn, M. Lu, Y. Wang, S.F. Lim, E.C. Cox, and R.H. Austin, P. Natl. Acad. Sci. USA. textbf102, 10012 (2005).
[3] N. Douville, D. Huh and S. Takayama, Anal. Bioanal. Chem. **391**, 2395 (2008).
[4] Y.M. Wang, J.O. Tegenfeldt, W. Reisner, R. Riehn, X. Guan, L. Guo, I. Golding, E.C. Cox, J. Sturm, and R.H. Austin, P. Natl. Acad. Sci. USA. **102**, 9796 (2005).
[5] P.G. de Gennes, *Scaling Concepts in Polymer Physics* (Cornell University Press, Ithaca, NY, 1979).
[6] T. Odijk, Macromolecules **16**, 1340 (1983).
[7] D.W. Schaefer, J.F. Joanny and P. Pincus, Macromolecules **13**, 1280 (1980).
[8] M. Daoud and P.G. Degennes, J. Phys. France **38**, 85 (1977).
[9] S. Jun, D. Thirumalai and B.Y. Ha, Phys. Rev. Lett. **101**, 138101 (2008).
[10] Y. Jung, S. Jun and B.Y. Ha, Phys. Rev. E Stat. Non-

linear Soft Matter Phys. 79, 061912 (2009).
[11] T.W. Burkhardt, J. Phys. A-Math. Gen. **28**, L629 (1995).
[12] J.B. Heng, A. Aksimentiev, C. Ho, P. Marks, Y.V. Grinkova, S. Sligar, K. Schulten and G. Timp, Nano. Lett. **5**, 1883 (2005).
[13] C.A. Merchant, K. Healy, M. Wanunu, V. Ray, N. Peterman, J. Bartel, M.D. Fischbein, K. Venta, Z. Luo, A.T.C Johnson and M. Drndic, Nano. Lett. **10**, 2915 (2010).
[14] J.T. Mannion, C.H. Reccius, J.D. Cross and H.G. Craighead, Biophys. J. **90**, 4538 (2006).
[15] M.M. Inamdar, W.M. Gelbart and R. Phillips, Biophys. J. **91**, 411 (2006).
[16] S.L. Levy, J.T. Mannion, J. Cheng, C.H. Reccius and H.G. Craighead, Nano Lett. **8**, 3839 (2008).
[17] J.P. Ebel, J.L. Anderson and D.C. Prieve, Langmuir. **4**, 396 (1988).
[18] P.O. Staffeld and J.A. Quinn, J. Colloid Interface Sci. **130**, 69 (1989).
[19] P.O. Staffeld and J.A. Quinn, J. Colloid Interface Sci. **130**, 88 (1989).
[20] T. Odijk, J. Chem. Phys. **125**, 204904 (2006).
[21] T. Su, S.K. Das, M. Xiao and P.K. Purohit, PLoS One, **6**, e16890 (2011).
[22] P. Nelson, *Biological physics: energy, information, life* (W. H. Freeman, NY, 2003).
[23] G. Sposito, *The chemistry of solids* (Oxford University Press, Oxford, UK, 1989)
[24] C. Brennen and H. Winet, Ann. Rev. Fluid Mech. **9**, 339 (1977).
[25] A.F. Voter, Introduction to the Kinetic Monte Carlo Simulation Method, in *Radiation effects in solids (NATO science series II: mathematics, physics and chemistry)* (Volume 235, 1-23, 2007).
[26] R. Raj and P.K. Purohit, Europhys. Lett. **91** 28003 (2010).
[27] D.F. Katz, J.R. Blake and S.L. Paveri-Fontana. J. Fluid Mech. **72** 529 (1975).
[28] C.W. Oseen, Neuere Methoden und Ergebnisse in der Hydrodynamik (Akademische Verlagsgesellschaft, Leipzig, 1927).
[29] E.R. Dufresne, D. Altman, and D.G. Grier, Europhys. Lett. **53**, 264 (2001).
[30] L. P. Faucheux and A. J. Libchaber, Phys. Rev. E **49**, 5158 (1994).
[31] B. Lin, J. Yu, and S. A. Rice, Phys. Rev. E **62**, 3909 (2000).
[32] J.F. Marko, E.D. Siggia, Macromolecules, **28**, 8759 (1995).
[33] D. Stigter, Biopolymers, **16**, 1435 (1977).
[34] P.E. Sottas, E. Larquet, A. Stasiak and J. Dubochet, Biophys. J. **77**, 1858 (1999).
[35] V.V. Rybenkov, N.R. Cozzarelli and A.V. Vologodskii, Proc. Natl. Acad. Sci. USA. **90**, 5307 (1993).
[36] J.W. Larson, G.R. Yantz, Q. Zhong, R. Charnas, C.M. D'Antoni, M.V. Gallo, K.A. Gillis, L.A. Neely, K.M. Phillips, G.G. Wong, S.R. Gullans and R. Gilmanshin, Lab Chip. **6**, 1187 (2006).
[37] S. Yip (Ed.), *Handbook of Materials Modeling* (Springer Science and Business Media, 2005).
[38] J. Wang and H. Gao, J. Mater. Sci. **42**, 8838 (2007).
[39] W.C.K. Poon and D. Andelman, *Soft Condensed Matter Physics in Molecular and Cell Biology* (CRC Press, Taylor & Fransic Group, Boca Ration, FL, 2006).
[40] J.W. Hatfield and S.R. Quake, Phys. Rev. Lett. **82**, 3548 (1999).
[41] J.T. Del Bonis-O'Donnell, W. Reisner and D. Stein, New. J. Phys. **11** 075032 (2009).
[42] R. Peters, Biochim. Biophys. Acta. **1793** 1533 (2009).
[43] M. Groll, M. Bochtler, H. Brandstetter, T. Clausen and R. Huber, Chembiochem **6** 222 (2005).
[44] K. Huang, *Statistical Mechanics* (John Wiley & Sons, Inc., New York, London, Sydney, 1963).
[45] T. Christen, J. Phys. D **40**, 5723 (2007).
[46] T. Odijk, Macromolecules. **19**, 2313 (1986).